

UC Berkeley

UC Berkeley Previously Published Works

Title

SimVascular: An Open Source Pipeline for Cardiovascular Simulation

Permalink

<https://escholarship.org/uc/item/2n51x320>

Journal

Annals of Biomedical Engineering, 45(3)

ISSN

0145-3068

Authors

Updegrave, Adam
Wilson, Nathan M
Merkow, Jameson
[et al.](#)

Publication Date

2017-03-01

DOI

10.1007/s10439-016-1762-8

Peer reviewed



Published in final edited form as:

Ann Biomed Eng. 2017 March ; 45(3): 525–541. doi:10.1007/s10439-016-1762-8.

SimVascular: An Open Source Pipeline for Cardiovascular Simulation

ADAM UPDEGROVE¹, NATHAN M. WILSON⁵, JAMESON MERKOW², HONGZHI LAN³, ALISON L. MARSDEN^{3,4}, and SHAWN C. SHADDEN^{1,6}

¹Department of Mechanical Engineering, University of California, Berkeley, CA, USA;

²Department of Electrical and Computer Engineering, University of California, San Diego, CA, USA;

³Department of Bioengineering, Stanford University, Palo Alto, CA, USA;

⁴Department of Pediatrics, Stanford University, Palo Alto, CA, USA;

⁵Open Source Medical Software Corporation, Santa Monica, CA, USA;

⁶University of California, Berkeley, CA 94720-1740, USA

Abstract

Patient-specific cardiovascular simulation has become a paradigm in cardiovascular research and is emerging as a powerful tool in basic, translational and clinical research. In this paper we discuss the recent development of a fully open-source SimVascular software package, which provides a complete pipeline from medical image data segmentation to patient-specific blood flow simulation and analysis. This package serves as a research tool for cardiovascular modeling and simulation, and has contributed to numerous advances in personalized medicine, surgical planning and medical device design. The SimVascular software has recently been refactored and expanded to enhance functionality, usability, efficiency and accuracy of image-based patient-specific modeling tools. Moreover, SimVascular previously required several licensed components that hindered new user adoption and code management and our recent developments have replaced these commercial components to create a fully open source pipeline. These developments foster advances in cardiovascular modeling research, increased collaboration, standardization of methods, and a growing developer community.

Keywords

Patient-specific modeling; Image-based CFD; Hemodynamics; Open-source

Address correspondence to Shawn C. Shadden, University of California, Berkeley, CA 94720-1740, USA. shadden@berkeley.edu.

CONFLICTS OF INTEREST

The authors do not have conflicts of interest relevant to this manuscript.

INTRODUCTION

Cardiovascular disease is the leading cause of death and disability worldwide. Central to both the causes and consequences of cardiovascular disease are local and regional disruptions in blood flow. The relationships between hemodynamics and cardiovascular diseases are subtle and multifaceted. While qualitative understanding and correlations are well documented,^{14,28,33,41,45,68} precise knowledge of hemodynamic conditions is needed to quantify risk and evaluate mechanisms. Simulation-based methods can provide a powerful framework in this regard. Advanced numerical methods are enabling increasingly realistic representations of cardiovascular physiology. Moreover, because the role of hemodynamics in any disease scenario is highly individualized, medical imaging and clinical data often forms the basis for patient-specific numerical simulations. These simulations can now provide a means to perform patient-specific treatment planning, virtual surgery and design optimization.

Image-based blood flow modeling was pioneered in the late 1990s and early 2000s^{23,39,40,48,60,62} and, in the years since, has proven to be a powerful tool in basic science and clinical research. Indeed, HeartFlow recently introduced the first FDA-approved simulation-based service for routine clinical evaluation of coronary stenoses.⁶¹ In most image-based modeling applications, 3D angiographic data obtained from computed tomography (CT) or magnetic resonance imaging (MRI) is used to construct a geometric model of a vascular region. Image processing is used to construct a vascular model that is then imported into a computational fluid dynamics (CFD) package to generate a volumetric mesh and numerically simulate blood flow. While numerous image processing software packages exist, most are not designed to generate computer models well-suited for simulation purposes. And while numerous CFD packages exist, most are not designed to accommodate the sophisticated boundary conditions, physiologic models and physics specific to cardiovascular modeling.

The software package SimVascular was originally developed in the lab of Charles Taylor at Stanford University to provide a complete pipeline from medical image data segmentation to patient specific blood flow simulation and analysis. SimVascular provides boundary conditions that achieve physiologic levels of pressure, fluid structure interaction, and a highly accurate and efficient finite element flow solver. The software was released in 2007, under a team including some of the present co-authors, and remained the only software package for cardiovascular simulation that includes the entire pipeline from model construction to simulation analysis. However, the need for commercial components and licenses previously hindered new user adoption and prevented complete open source release. Moreover, the infrastructure for continued software development was lacking as well as necessary features for wider use.

To overcome the above barriers, the SimVascular revitalization project was launched in 2013. A major goal of these efforts was the development and integration of open source alternatives for a truly open source SimVascular project. In addition, new functionality in nearly all facets of the pipeline has been added to enhance modeling accuracy, usability and efficiency. Examples of recent enhancements include direct 3D segmentation, discrete solid

modeling, mesh repair tools, fluid-solid interaction with variable wall properties, closed-loop lumped parameter network modeling, and GUI updates. In addition, case studies, online documentation, CMake compatibility, a user forum, binary packages for all major operating systems, and other infrastructure to support the open source project have been brought online (www.simvascular.org). In this paper we describe the main features of the SimVascular software and briefly demonstrate its application to publicly available sample case studies.

METHODS

SimVascular Architecture and Maintenance

The source code is built upon a *repository* in which objects are stored, maintained, and tracked. The repository, which is a large hash table, facilitates memory management across the large scale software platform. The repository stores all data structures as a *cvRepositoryData* object. Figure 1 displays a simplified inheritance diagram for the SimVascular data structures. Stemming from the *cvRepositoryData* data structure, there are several objects used within SimVascular's source code for data representation. These objects include *cvDataObject* (a general subclass of *cvRepositoryData*), *cvSolidModel*, and *cvMeshObject*. These are abstract base classes providing virtual functions for implementation in derived classes. They define a rigid structure for the derived classes that is important for the modularity of SimVascular. SimVascular uses external libraries for multiple Solid Model and Mesh Object classes (Fig. 1). Each of these packages are included in a derived class demonstrating SimVascular's extensibility for new module plugins.

The source code is maintained as a repository on github (www.github.com/SimVascular). Maintenance and development is enhanced with multiple modern software development tools. CMake is used to build and test functionality of the source, while Travis CI is used for automated building on various versions of Linux with different library versions. Stable binary releases of the software are posted on Simtk (www.simtk.org/home/simvascular). Simtk also currently hosts user forums, email lists, and a bug tracker for SimVascular.

The SimVascular Pipeline

The SimVascular pipeline starts with image processing and segmentation and continues all the way through to post-processing of simulation results. Figure 2 displays nominal steps of image-based modeling in SimVascular, although alternative and additional steps may be employed. The GUI is comprised of an interactive display, as well as image and work tabs (Fig. 3). The image tabs provide control over how the image data is displayed. This includes functionality such as loading medical image data, point cloud visualization, and volume rendering. The work tabs encapsulate the core functionality of the model construction process. We briefly describe the main steps in the pipeline, and then provide additional details in the subsequent sections.

Paths—The segmentation process typically starts by creating pathlines along the vessels of interest. It is possible to create models using a *lofted 2D* segmentation method (“2D Segmentation Methods” in section) or *direct 3D* segmentation methods (“3D Segmentation

Methods” in section). When performing lofted 2D segmentation, the pathlines are used to resample the image data to a cross-sectional “intensity probe” window that can be moved along the vessel’s path (Fig. 4a). For direct 3D segmentation methods, paths are not necessary but can be used to help initiate region growing methods.

Segmentation—For the lofted 2D segmentation method, functionality is provided to move along each pathline and create a series of segmentations that delineate the luminal boundaries of the vessel (Fig. 4b). Alternatively, for direct 3D segmentation, functionality is provided to position seed surfaces (spheres) that will expand, merge and morph in 3D space to fill in the luminal boundary.

Model—After image segmentation, a solid model can be generated. Following the lofted 2D approach, the series of segmentations are lofted together with splines (Fig. 4c). For either the lofted 2D or direct 3D approach, functionality for manipulating the model and identifying faces of the model (e.g., for specifying boundary conditions) is provided. Additionally, surfaces from 2D (Fig. 4d) and 3D methods can be combined into a single model using custom boolean operations.

Meshing—The meshing tab provides functionality to create a volumetric mesh of the model for subsequent computational modeling. SimVascular supports construction of unstructured tetrahedral meshes as well as several advanced meshing features including boundary layer meshing, radius-based meshing, regional refinement and adaptive meshing.

Simulations—The simulation tab includes three steps, in which a presolver, solver and postsolver are used to generate simulation results. There is functionality to assign boundary conditions, material properties, and set parameters for the solver. The svSolver can be run through the GUI; however, it is common for simulation files to be generated on a desktop computer and then copied to a high performance computing (HPC) cluster where the svSolver can be run in parallel.

Console—SimVascular contains an interpreter in which C++ functions bound by Tcl (or Python) can be called interactively through a command line console. This gives users the ability to use custom scripts, in addition to or in place of the GUI, to access a wide range of the SimVascular functionality and automate repeatable procedures.

Image Segmentation

Image data provides a set of scalar values defined on a structured grid. The data defines an intensity field in 3D space and objects or material within the image are identified by different intensity values or ranges. The first step in image-based modeling is to segment the image data in a region of interest (ROI) to extract the boundary or structure of an object from the intensity field. With SimVascular, the segmentation process is most commonly used to identify the luminal surface of a blood vessel; however other anatomical structures may be similarly segmented and modeled. Extensive research has been conducted in the field of image segmentation^{7,30,32,67} and SimVascular utilizes established techniques that incorporate both 2D and 3D image segmentation techniques.

2D Segmentation Methods

Figure 4 displays the steps to generate an individual vessel using the lofted 2D segmentation approach. First, an approximate centerline is generated along the vessel (Fig. 4a). Along this path, a series of segmentations is generated by stepping a 2D cross-sectional imaging window along the vessel (Fig. 4b). Finally, the segmentations are lofted together to give a surface representing the lumen (Fig. 4c). Lofting is performed through generation of spline interpolating functions. To create a vascular network, multiple vessels are created sequentially, and then unioned via a set of boolean operations (Fig. 4d).

The 2D cross-sectional imaging window (Figs. 4a, 4b) is limited to a region around the path so that peripheral image data does not interfere with the local segmentation of the vessel of interest. There are a variety of methods implemented to segment the lumen, though the two main approaches are based on level set and threshold techniques.

Level Set—A contour is initialized by a seed point (small disk) and grows in the directions of changing intensity values to find the location of sharpest change. This picks out the vessel wall as a complete contour region (Fig. 5, left). A pair of windows displaying the image intensity and magnitude of the intensity gradient facilitates segmentation creation and editing. A moving level set front is governed by

$$\phi_t = -v|\nabla\phi| - \nabla\mathbf{g} \cdot \nabla\phi, \quad (1)$$

where ϕ_t represents the front, v is the velocity normal to the front, and \mathbf{g} is an edge detection function. The velocity term, v , is represented differently for two different stages. In the first stage, the velocity is represented by exponentially decaying functions. In the second stage, the velocity is represented by edge attraction functions. Parameters in the SimVascular GUI correspond to scalars governing the decay in the first stage and attraction in the second stage. For more details, see Ref. 67.

Threshold—Image intensity values are assumed to be centered at each pixel. A bilinear interpolation function is then used to create isocurves of a specified threshold value on the image. These isocurves are potential contours of the lumen. A circle of specified radius is centered on the path, and the smallest closed isocurve that completely encapsulates the circle is identified as the lumen boundary (Fig. 5, right).

Manual—Manual segmentation is useful for noisy data sets, images with complicated features, or cases where the automated methods fail to converge. Points along the lumen are manually selected by the user and (automatically) connected with a closed spline to represent the geometry.

Analytic—A 2D segmentation is created using a circle or ellipse of user specified dimensions. This can be helpful for ideal geometries, noisy data, or locations where no image data exists.

Segmentations created by any of the above methods can be smoothed post creation. Also, in some applications multiple segmentations can be created using the same set of level set or threshold parameters, allowing for “batch mode” segmentation. In batch mode, for a specified range along the vessel path, segmentations are automatically generated with specified settings. Segmentations can then be checked and modified as needed using the editing or smoothing tools provided in SimVascular. In cases of appropriate image quality, this can be an efficient way to automatically generate a set of segmentations along each path.

3D Segmentation Methods

Direct 3D segmentation methods are also available in SimVascular, which are useful for segmenting vessel sections that do not lend themselves well to 2D cross section segmentation, such as aneurysms, and vessel junctions. This process begins by placing 3D seed “points” (small spheres) within vascular locations. These act as initial surfaces for active contours and level set algorithms. Seeds can be positioned by manual selection in the 3D window using coordinate position sliders, or along SimVascular pathlines.

In addition to specification from seeds, initial contours from which a 3D surface is grown can be specified via several alternative methods. These methods include initialization from previous level set surfaces, surfaces created through 2D segmentation, and even 3D iso-surfaces of the image data. After positioning seed points or selecting an initial contour surface, a 3D surface is grown using one of two level set algorithms: (1) a Laplacian fast edge grower, or (2) a geodesic smoothing level set. Both level set types are implemented by modifying the terms in Eq. (1). These level set algorithms propagate segmentation labels through an energy minimization of appearance, curvature, and propagation terms. Appearance features are controlled by modifying the parameters shown in the following equation:

$$E = \frac{1}{1 + (\Delta(I * f) \cdot \kappa)^m} \quad (2)$$

where $*$ is the convolution operator, f represents a Gaussian smoothing kernel, and k and m represent contrast parameters for contrast scaling and proximity.

Model Creation

The segmentation process results directly, or indirectly, in a *boundary representation* of the blood flow domain (or other physical region of interest). The output of the 3D segmentation process is a triangulated surface that serves as a discrete boundary representation. For the lofted-2D segmentation approach, the segmentations must be lofted to construct a solid model as described below, which can be represented as either a triangulated surface, or analytic (CAD) model. Additional procedures are often needed to make the solid model compatible with computational modeling. SimVascular supports four different solid modeling approaches: (1) PolyData, (2) OpenCASCADE, (3) Parasolid, and (4) Discrete.

PolyData—The most extensive solid modeling package in SimVascular is PolyData. Combining custom-developed procedures with filters available in VTK (www.vtk.org) and VMTK (www.vmtk.org), the PolyData kernel provides multiple ways to create and manipulate a geometry. The PolyData kernel is first used to generate a model from the ordered 2D segmentations. Splines are formed along the length of the vessel that connect the 2D segmentations, resampled to a specified number of points, and then connected and triangulated to form a complete PolyData surface. Each set of segmentations results in one lofted vessel. Additional lofted vessels are then combined using an ordered Boolean addition. A customized Boolean operation for triangular surfaces is used for this operation.⁶⁵ Other PolyData operations provided in SimVascular include smoothing, blending, decimation, subdivision, trimming, deleting cells, and filling holes. Many of these are available as localized operations, which can confine operations to a subset of the model. Selection options include picking a spherical region, using single or multiple faces, identifying the region between two faces (e.g., vessel junctions), or even clicking on individual cells on the model.

A PolyData model is an unstructured triangulated surface. Discrete models generated in other segmentation programs (e.g. in STL format) can be imported into the SimVascular modeling pipeline as a PolyData model (Fig. 6). After importing, one can identify faces of the discrete model and perform the same set of operations that are available for models created in SimVascular.

OpenCASCADE—The OpenCASCADE (www.open-cascade.org) modeling kernel provides 3D solid modeling functionality found in most CAD software. OpenCASCADE is the solid modeling package utilized in FreeCAD (www.freecadweb.org). Using this component, one can use SimVascular to create a CAD model by lofting the 2D segmentations into a Non-Uniform Rational B-Spline (NURBS) surface. As an analytic surface, such a model lends well to typical CAD procedures such as blending, cutting, and Boolean operations. These functions are accessible through SimVascular's GUI and console.

Parasolid—Parasolid (Siemens PLM Software, Plano, TX, USA) is an *optional* licensed solid modeling plugin, which is the solid modeling package utilized in SolidWorks (www.solidworks.com). Using this licensed component, one can also perform lofting of 2D segmentations into a NURBS surface and access typical CAD procedures through SimVascular's GUI and console. In general, much of the functionality between Parasolid and OpenCASCADE is similar; however, Parasolid has generally been found to be more robust.

Discrete—The last solid modeling package, Discrete, is an *optional* plugin that simply provides a way to represent a discrete PolyData surface as a model that is usable by SimVascular's commercial mesher, MeshSim (Simmetrix, Inc., Clifton Park, NY, USA).

At the end of the model creation step, faces on the model are labeled with a user specified name and identifier (*ModelFaceID*). These identifiers can later be used to specify boundary conditions or material properties in the simulation steps. When a model is created using 2D or 3D segmentation approaches in SimVascular, names and *ModelFaceIDs* are automatically prescribed. Customized naming and prescription of faces can be accomplished using built in

functionality, which is also helpful if the model is created using an external program and imported into SimVascular.

Meshing

After image segmentation and model construction, the next step for image-based blood flow modeling is discretizing the volumetric domain through mesh generation. The most robust meshing packages have traditionally been commercial codes, though in the past decade, high quality open source meshing tools have also become available.

SimVascular supports two meshing kernels for the user to choose from: (1) TetGen and (2) MeshSim. The open-source TetGen kernel is actually a combination of functionality from TetGen (www.tetgen.org), as well as custom code for adaptive meshing, code from VMTK (www.vmtk.org) for boundary layer meshing and radius-based meshing, and MMG (www.mmgtools.org) for fast and robust surface remeshing. The optional MeshSim kernel is a licensed mesher by Simmetrix (www.simmetrix.com). Both MeshSim and TetGen kernels provide a broad and similar range of meshing options (Fig. 7). Surface remeshing, local mesh refinement, and cylindrical mesh refinement are a few of the options available in both packages. Boundary layer meshing is supported, which enables smaller, thinner elements over near-wall regions where the gradient of the velocity normal to the surface changes most drastically. Also mesh adaption based on *a-posteriori* error estimates is supported to provide a more efficient discretization strategy. This is achieved by computing the second directional derivative, or the Hessian, of the solution (e.g., blood velocity magnitude). The eigenvalues of this Hessian matrix at each mesh point are used as an indication of how much the solution is changing around this point, and the mesh is locally refined/coarsened accordingly.⁵¹

Simulation

The meshing procedure produces an unstructured volumetric mesh that can be used as the computational domain for simulation of blood flow and pressure. The SimVascular simulation module includes three parts: (1) Presolver (svPre), (2) Flowsolver (svSolver), and (3) Postsolver (svPost).

Boundary Conditions—Boundary conditions are essential to obtaining valid, physiologically realistic cardiovascular simulation results. The foremost boundary condition is the traction (no-slip, no-penetration) boundary condition applied at the lumen surfaces (“walls”). The other boundaries can be considered inflow (“inlet”) and outflow (“outlet”) boundaries, and it is important that boundary conditions specified on these surfaces represent the physiology of the vasculature outside the 3D computational domain. For example, boundary conditions are essential for obtaining realistic values of pressure required for accurate fluid structure interaction simulations. SimVascular provides different options for boundary condition assignment at the three boundary types. Dirichlet or Neumann boundary conditions can be applied at either inlets or outlets of the model, which enables a broad range of options for boundary condition specification. These values can be directly prescribed, or implicitly prescribed from reduced order models of the upstream or downstream vasculature. Along these lines, inflow and outflow boundary conditions can be prescribed in an “open-loop” or “closed-loop” manner (Fig. 8). For the latter, inflow

conditions become coupled to the dynamics of the model itself, which can be necessary in surgical planning applications where one virtually changes the vascular geometry in a manner that may alter inflow conditions from the nominal or measured values.

Inlets—At the inlet (or inlets), a flow rate or pressure waveform is typically prescribed. The waveform is fit to a truncated Fourier series so that the flow rate (or pressure) at arbitrary time points can be queried. When a volumetric flow rate is specified, it is mapped to the inlet plane using a specified profile; plug, parabolic and Womersley profiles are currently supported in SimVascular. This mapping can account for non-circular inlet planes. In addition, SimVascular supports the ability to map planar phase contrast magnetic resonance imaging (PCMRI) velocity measurements to the inlet plane of the model for scenarios where such measurements are available.⁷⁰

Outlets—There are a number of techniques used in SimVascular for outflow boundary conditions that model the effects of the downstream vasculature, including impedance boundary conditions, Wind-kessel-type boundary conditions (resistance, RC circuit, RCR circuit, etc), and more complicated lumped parameter network (LPN) models like coronary boundary conditions.²² These boundary conditions effectively model the pressure-flow relationship at each outlet due to the respective downstream vascular bed. Impedance and Windkessel-type boundary conditions are coupled implicitly to the 3D computational domain by prescribing pressure in a weak manner in the flowsolver as described in detail in Ref. 66. In addition, the coupled LPN network can be modified without needing to recompile the solver, thus making it very simple to implement a variety of boundary conditions.

We can view outlet boundary conditions as being specified by a lumped parameter (LP) model of the downstream vascular domain. Unlike distributed models (such as the 3D computational domain) that are governed by PDEs, LP models are governed by ODEs. Therefore, providing the ability to couple ODEs that represent the dynamics of the downstream vascular domain opens vast possibilities for modeling downstream physiology. In fact, such models can represent the entirety of the circulation outside the 3D computational domain, in which case one achieves a “closed-loop” model and the ODEs serve to both modulate outflow conditions and inflow conditions (Fig. 8, right). Except for very simple LP models, the ODEs cannot be solved analytically, and must be solved numerically. For such couplings, SimVascular contains an efficient and stable numerical scheme for implicitly coupling ODE models with the flowsolver for the 3D domain without significantly increasing the overall simulation cost,^{18,35} which has been used in several recent applications.^{25,54}

Walls—No-penetration, no-slip boundary conditions are applied for rigid wall simulations. Alternatively, the flowsolver can be used to model fluid structure interaction (FSI). For FSI simulations, the fluid and solid domains are coupled using the coupled momentum method (CMM),¹⁹ with the wall modeled as a linear elastic material, which can have uniform or variable elastic modulus and thickness along each vessel.

Solver Methodology—Blood flow is modeled using the incompressible Navier-Stokes equations,

$$\begin{aligned} \rho \dot{v}_i + \rho v_j v_{i,j} - p_{,i} - \tau_{ij,j} &= 0, \\ v_{i,j} &= 0, \end{aligned} \quad (3)$$

where ρ is blood density, v_i is the i th component of the fluid velocity and \dot{v}_i its time derivative, p is the pressure, and τ_{ij} is the viscous portion of the stress tensor. The flowsolver inside of SimVascular evolved from the academic finite element code PHASTA (Parallel, Hierarchical, Adaptive, Stabilized, Transient Analysis) for solving the Navier-Stokes equations in an arbitrary domain with the streamline-upwind/Petrov-Galerkin (SUPG) and pressure-stabilizing/Petrov-Galerkin (PSPG) methods.⁶⁹

The SUPG/PSPG formulation is defined on the finite-dimensional trial solution and weight function spaces \mathbf{S}_h^k , \mathbf{W}_h^k , and P_h^k . The domain is denoted by $\Omega \in \mathbb{R}^3$, and its boundary by $\Gamma = \Gamma_D \cup \Gamma_N$. Dirichlet boundary conditions are applied on Γ_D and, Neumann, or flux type, boundary conditions are applied on Γ_N . Ω is discretized by n_{el} linear elements, Ω_e . The weak form of Eq. (3) becomes

$$\begin{aligned} B_G(w_i, q; v_i, p) &= \int_{\Omega} \left\{ w_i (\rho \dot{v}_i + \rho v_j v_{i,j}) \right. \\ &+ w_{i,j} (-p \delta_{ij} + \tau_{ij}) - q_{,i} v_i \left. \right\} d\Omega \\ &+ \int_{\Gamma_N} \{ w_i (p \delta_{in} - \tau_{in}) + q v_{in} \} d\Gamma = 0, \end{aligned} \quad (4)$$

where $\mathbf{w} \in \mathbf{W}_h^k$ and $q \in P_h^k$.

Momentum stabilization is required for advection dominated flows, and pressure stabilization is otherwise required to support the use of linear tetrahedral elements (P1–P1) in the SimVascular flowsolver for velocity and pressure, which is computationally efficient in terms of memory and mesh size. The following stabilized weak form is thus considered

$$\begin{aligned}
 B(w_i, q; v_i, p) &= \underbrace{B_G(w_i, q; v_i, p)}_{\text{Eq.4}} \quad (5) \\
 &+ \sum_{e=1}^{n_{el}} \int_{\Omega_e} \left\{ \underbrace{\tau_M (v_j w_{i,j} + q_{,i}) L_i}_{\text{momentum and pressure stabilization}} \right. \\
 &+ \left. \underbrace{\tau_C w_{i,i} v_{j,j}}_{\text{incompressibility constraint stabilization}} \right\} d\Omega \\
 &+ \sum_{e=1}^{n_{el}} \int_{\Omega_e} \left\{ \underbrace{w_i \bar{v}_j v_{i,j} + \bar{\tau} \bar{v}_j w_{i,j} \bar{v}_k v_{i,k}}_{\text{compensation for the stabilization terms}} \right\} \\
 d\Omega &= 0,
 \end{aligned}$$

where $\mathbf{w} \in \mathbf{W}_h^k$ and $q \in P_h^k$. L_i represents the residual of the i th momentum equation,

$$L_i = \dot{v}_i + v_j v_{i,j} + p_{,i} - \tau_{ij,j}. \quad (6)$$

This formulation includes both the momentum and pressure stabilization,²⁰ which are controlled by the stabilization parameter, τ_M . The incompressibility constraint is also stabilized and is controlled by the stabilization parameter, τ_C . The addition of these stabilization terms causes inconsistencies in the conservation of momentum, so Taylor *et al.*⁶³ introduced the final term of the weak form to compensate for the momentum imbalance. For further details, see Ref. 69.

The above weak form contains stabilization terms for momentum, pressure, and the incompressibility constraint. In addition, backflow stabilization as described in¹⁵ has been added to the SimVascular solver to prevent instabilities at Neumann boundaries that may experience backflow due to flow reversal (either total reversal due to conservation of mass, or partial reversal due to vortical structures near the outlet). This backflow stabilization method has been shown to provide a more robust and effective way to deal with numerical divergence caused by flow reversals at Neumann boundaries compared to more common methods.¹⁵

The stabilized FEM formulation of Navier Stokes is discretized in time using the generalized alpha time-stepping scheme in the SimVascular flowsolver. A recently developed linear solver with specialized preconditioners tailored to handle large vascular resistances coupled at outflow boundaries is used to handle cardiovascular simulations and reduce solution time,¹⁶ providing an alternative to the original commercial linear solver LesLib (Altair, Inc.,

Mountain View, CA). The flowsolver can be run with a single core or with multiple cores using the Message Passing Interface (MPI). A related version of the flowsolver has demonstrated excellent scalability on large clusters,⁷² which can enable the study of transiently or transitionally turbulent flow conditions.

Hemodynamics Analysis—SimVascular can post-process the simulation files to extract or calculate relevant hemodynamic quantities such as velocity, pressure, wall shear stress (WSS), and oscillatory shear index. Files can be exported to VTK formats to facilitate visualization of the data in leading open source scientific visualization softwares such as ParaView and VisIt, as well as more custom postprocessing by applying VTK classes and filters, which can be scripted using Python. For example, recent studies have analyzed flow fields produced by SimVascular to compute Lagrangian coherent structures,^{3,4,6,55} residence times in aneurysms,^{57,58} turbulent kinetic energy,^{1,29} particle tracking,^{43,46} and to model surface transport processes relevant for thrombosis.^{2,21}

RESULTS

Case Studies and Validation

SimVascular has been used in a wide range of applications from studying blood flow in the heart, brain, and lungs and for various disease and surgical planning scenarios (e.g., Ref. 1, 5, 8, 11, 17, 31, 36, 44, 52 among others). *In vitro* validation in the thoracic aorta compared flow measurements from PCMRI in deformable phantoms to SimVascular FSI simulations.²⁷ The average difference between measured and simulated flow was approximately 13% (mean), which is within the reported 10% accuracy of PCMRI flow measurements. The difference between the measured and simulated mean pressure was approximately 1.8%. Similar validation efforts were carried out in the coronary arteries and found similar agreement between measured and simulated flows.²⁶ *In vivo* validation has been performed by comparing fluctuating/turbulent kinetic energy computations obtained with SimVascular with measurements obtained using 4D flow imaging in aortic coarctation in Ref. 1 as shown in Figure 9. In that study the quantified mean differences between *in vivo* measurements and CFD predictions of fluctuating kinetic energy were on the order of 10% and within expectations due to modeling and measurement errors. In addition, *in vivo* measurements of flow velocities in abdominal aortic aneurysms were shown in Ref. 3 to compare well to computations obtained using SimVascular, and simulated predictions of flow in Y-graft Fontan procedures were compared to *in vivo* clinical data in Ref. 71. SimVascular has also been used in several recent CFD challenges for image-based hemodynamics modeling, e.g. Ref. 56. Moreover, simulation-derived designs from SimVascular have been translated to clinical use, an example of which is the pilot study of the Fontan Y-graft.^{34,37}

As a compelling exposition of SimVascular's application to image-based hemodynamics modeling, the Open Source Medical Software Corporation (OSMSC) has compiled models and results from over 100 unique studies using SimVascular (Fig. 10). Figure 11 breaks down the contents of the cardiovascular and pulmonary model repository available to users at www.vascularmodel.com. We briefly present the results from two of these studies, as well

as an example where FSI has been used for simulation of a coronary artery bypass graft (CABG).

Pulmonary Arteries

The pulmonary arteries supply blood from the heart to the lungs for oxygenation. Pulmonary arterial hypertension (PAH) and pulmonary embolisms are common diseases associated with the pulmonary arteries. Image data from a woman aged 67 was used to construct an extensive model of the pulmonary arteries from the main pulmonary artery to various levels of branching in the left and right pulmonary pathways (Fig. 13). A total of 100 arteries were modeled. The inflow waveform was adapted from Ref. 12 to represent a typical resting pulmonary waveform. Resistance boundary conditions were used at all outlets. Resistance values were distributed inversely to outlet area and with total values chosen to match physiologic flow splits and pulmonary pressures. Wall shear stress values in the proximal arteries were observed to match values in previous studies, and flow rates through the main pulmonary arteries were consistent with measured values from PCMRI.⁴² This application was used to evaluate wall shear stress and other quantities in normal and PAH patient specific models, revealing significant differences between healthy and diseased states, which helped to reveal mechanisms for PAH progression.⁵⁹

Aortic and Femoral Arteries

The second example is a model extending from the aortic root to the femoral arteries (Fig. 12). This model was constructed from a large CT dataset of a 21-year old female subject. The aortic inflow waveform was taken from Ref. 47 and averaged to a mean cardiac output of 4.6 L/min. Three element Windkessel models were applied at each outlet with resistances and capacitances tuned to achieve desired flow distribution amongst the various outlets and physiologic pressure pulse. Various literature sources were used to support the distribution ratios to each model outlet. For example, 13% of the cardiac output was distributed to the carotid arteries, 65% to the descending thoracic aorta, and 22% to the subclavian arteries. Descending thoracic flow was further divided to the remaining arterial beds based on target flow rates from the literature. Target arterial pressures were based on typical pressures for a young healthy adult. The simulation results match a target diastolic pressure of 80 mmHg and systolic pressure of 120 mmHg.

Coronary Artery Bypass Graft

Coronary artery bypass graft surgery is performed in roughly 400,000 patients annually in the United States.¹⁰ Vein graft failure continues to be a major clinical challenge in patients post CABG surgery. Simulations including material wall properties and vessel wall deformation may give insight into flow and wall mechanics leading to vein graft failure and optimal choice of surgical method. In this example, a model including the aorta, the coronary arteries, and the graft were constructed from CT images with SimVascular. Vessel wall thickness and material properties were prescribed based on literature values.^{13,50} For the boundary conditions at the aortic inlet and outlet, a closed-loop LPN was used that included circuit blocks for the heart, the systemic circulation, and the coronary circulation. Because flow in the coronary arteries is out of phase with the systemic circulation, coronary specific boundary conditions were applied at each of the coronary artery outlets. The model

was tuned to send 4% of the cardiac output to the coronary arteries.⁹ In addition, target pressures and flow splits were matched using values taken from literature. Velocity during end diastole and wall displacement during peak systole are displayed in Figure 14. Significant differences in biomechanical conditions between venous and arterial grafts were identified.⁴⁹

DISCUSSION

SimVascular provides a complete pipeline for image-based hemodynamics simulation. Many custom features have recently been developed to enable efficient and flexible computer model construction from medical image data. While this software has benefited from more than a decade of development and use in state-of-the-art cardiovascular modeling research studies, the recent redevelopment of SimVascular has expanded and hardened its functionality and ease of use. Moreover, these recent efforts have made SimVascular completely open source, documented, and available on all major operating systems, which enables community use for research and education for the first time.

Because geometric fidelity and boundary conditions are of critical importance in accurate cardiovascular simulation, new features have focused on providing enhanced functionality for model construction, manipulation, and repair, as well as the specification and numerical treatment of physiologic boundary conditions, multidomain modeling, and fluid structure interaction. Many of these features are not possible in other softwares. The SimVascular solver has undergone significant development to include support for multiscale boundary conditions, backflow stabilization, and a new linear solver with specialized preconditioning to improve performance. Significant efforts have also been made to refactor and harden the SimVascular code for stable releases and standardized development.

SimVascular is an active software project undergoing continuous progression with further enhancements forthcoming. Currently, a new graphical user interface is being constructed in a modern framework with Qt and Python. The framework is built upon the Medical Imaging Interaction Toolkit (MITK; www.mitk.org) to facilitate handling and processing of image data. In addition, new methods for image segmentation based on machine learning and artificial neural networks are in development.³⁸ These methods will provide users with improved and automated image-to-model capabilities to reduce the time to construct accurate image-based models. In addition, modules for optimization, uncertainty quantification, and parameter estimation to match clinical data are under development.^{53,64} Lastly, new algorithms to convert a discrete model (typical output of direct 3D segmentation methods) to an analytic model (CAD standard) are being developed, and will enable users to import/export models that are editable in most CAD frameworks.

ACKNOWLEDGMENTS

This work was supported by the National Science Foundation SI2 program (Award No. 1407834 and 1562450) and in part by the NIH (Contract HHSN268201100035C).

REFERENCES

1. Arzani A, Dyverfeldt P, Ebberts T, and Shadden SC (2012) In vivo validation of numerical prediction for turbulence intensity in an aortic coarctation. *Ann. Biomed. Eng* 40(4):860–870. [PubMed: 22016327]
2. Arzani A, Gambaruto AM, Chen G, and Shadden SC. Lagrangian wall shear stress structures and near wall transport in high schmidt aneurysmal flows. *J. Fluid Mech* 790:158–172, 2016.
3. Arzani A, Les AS, Dalman RL, and Shadden SC. Effect of exercise on patient specific abdominal aortic aneurysm flow topology and mixing. *Int. J. Numer. Methods Biomed. Eng* 30(2):280–295, 2014.
4. Arzani A, and Shadden SC. Characterization of the transport topology in patient-specific abdominal aortic aneurysm models. *Phys. Fluids (1994-present)* (1994), 24(8):081901, 2012.
5. Arzani A, Suh GY, Dalman RL, and Shadden SC. A longitudinal comparison of hemodynamics and intraluminal thrombus deposition in abdominal aortic aneurysms. *Am. J. Physiol. Heart Circ. Physiol* 307(12):H1786–H1795, 2014. [PubMed: 25326533]
6. Astorino M, Hamers J, Shadden SC, and Gerbeau J. A robust and efficient valve model based on resistive immersed surfaces. *Int. J. Numer. Methods Biomed. Eng* 28(9):937–959, 2012.
7. Bezdek JC, Hall LO, and Clarke LP. Review of MR image segmentation techniques using pattern recognition. *Med. Phys* 20(4):1033–1048, 1992.
8. Bockman MD, Kansagra AP, Shadden SC, Wong EC, and Marsden AL. Fluid mechanics of mixing in the vertebrobasilar system: *Cardiovasc. Eng. Technol* 3(4):450–461, 2012.
9. Bogren HG, Klipstein RH, Firmin DN, Mohiaddin RH, Underwood SR, Rees RSO, and Longmore DB. Quantitation of antegrade and retrograde blood flow in the human aorta by magnetic resonance velocity mapping. *Am. Heart J* 117(6):1214–1222, 1989. [PubMed: 2729051]
10. Braunwald E, Antman EM, Beasley JW, Califf RM, Cheitlin MD, Hochman JS, Jones RH, Kereiakes D, Kupersmith J, Levin TN, et al. *Acc/aha 2002 guideline update for the management of patients with unstable angina and non-st-segment elevation myocardial infarction—summary article: a report of the american college of cardiology/american heart association task force on practice guidelines (committee on the management of patients with unstable angina)*. *J. Am. Coll. Cardiol* 40(7):1366–1374, 2002. [PubMed: 12383588]
11. Carr IA, Nemoto N, Schwartz RS, and Shadden SC. Size-dependent predilections of cardiogenic embolic transport. *Am. J. Physiol. Heart Circ. Physiol* 305(5):H732–H739, 2013. [PubMed: 23792681]
12. Cheng CP, Herfkens RJ, Taylor CA, and Feinstein JA. Proximal pulmonary artery blood flow characteristics in healthy subjects measured in an upright posture using MRI: the effects of exercise and age. *J. Magn. Resonance Imaging* 21(6):752–758, 2005.
13. Coogan JS, Humphrey JD, and Figueroa CA. Computational simulations of hemodynamic changes within thoracic, coronary, and cerebral arteries following early wall remodeling in response to distal aortic coarctation. *Biomech. Model. Mechanobiol* 12(1):79–93, 2013. [PubMed: 22415052]
14. Davies PF, Civelek M, Fang Y, and Fleming I. The atherosusceptible endothelium: endothelial phenotypes in complex haemodynamic shear stress regions in vivo. *Cardiovasc. Res* 99(2):315–327, 2013. [PubMed: 23619421]
15. Esmaily-Moghadam M, Bazilevs Y, Hsia T-Y, Vignon-Clementel IE, and Marsden AL. A comparison of outlet boundary treatments for prevention of backflow divergence with relevance to blood flow simulations. *Comput. Mech* 48:277–291, 2011.
16. Esmaily-Moghadam M, Bazilevs Y, and Marsden AL. A new preconditioning technique for implicitly coupled multidomain simulations with applications to hemodynamics. *Comput. Mech* 52:1141–1152, 2013.
17. Esmaily-Moghadam M, Hsia T-Y, and Marsden AL. The Assisted Bidirectional Glenn: a novel surgical approach for first stage single ventricle heart palliation. *J. Thorac. Cardiovasc. Surg* 149(3):699–705, 2015. [PubMed: 25454920]
18. Esmaily-Moghadam M, Vignon-Clementel IE, Figliola R, and Marsden AL. A modular numerical method for implicit 0D/3D coupling in cardiovascular finite element simulations. *J. Comput. Phys* 244:63–79, 2013.

19. Figueroa CA, Vignon-Clementel IE, Jansen KE, Hughes TJR, and Taylor CA. A coupled momentum method for modeling blood flow in three-dimensional deformable arteries. *Comput. Methods Appl. Mech. Eng* 195:5685–5706, 2006.
20. Franca LP and Frey SL. Stabilized finite element methods: II. The incompressible navier-stokes equations. *Comput. Methods Appl. Mech. Eng* 99(2–3):209–233, 1992.
21. Hansen KB, and Shadden SC. A reduced-dimensional model for near-wall transport in cardiovascular flows. *Biomech. Model. Mechanobiol* 15(3):713–722, 2016. [PubMed: 26298313]
22. Kim HJ, Vignon-Clementel IE, Coogan JS, Figueroa CA, Jansen KE, and Taylor CA. Patient-specific modeling of blood flow and pressure in human coronary arteries. *Ann. Biomed. Eng* 38(10):3195–3209, 2010. [PubMed: 20559732]
23. Krams R, Wentzel JJ, Oomen JAF, Vinke R, Schuurbiers JCH, De Feyter PJ, Serruys PW, and Slager CJ. Evaluation of endothelial shear stress and 3D geometry as factors determining the development of atherosclerosis and remodeling in human coronary arteries in vivo Combining 3D reconstruction from angiography and IVUS (ANGUS) with computational fluid dynamics. *Arterioscler. Thromb. Vasc. Biol* 17(10):2061–2065, 1997. [PubMed: 9351372]
24. Ku DN, Giddens DP, Zarins CK, and Glagov S. Pulsatile flow and atherosclerosis in the human carotid bifurcation. positive correlation between plaque location and low oscillating shear stress. *Arterioscler. Thromb. Vasc. Biol* 5(3):293–302, 1985.
25. Kung EO, Baretta A, Baker C, Arbia G, Biglino G, Corsini C, Schievano S, Vignon-Clementel IE, Dubini G, Pennati G, et al. Predictive modeling of the virtual Hemi-Fontan operation for second stage single ventricle palliation: two patient-specific cases. *J. Biomech* 46(2):423–429, 2013. [PubMed: 23174419]
26. Kung EO, Kahn AM, Burns JC, and Marsden AL. In vitro validation of patient-specific hemodynamic simulations in coronary aneurysms caused by Kawasaki disease. *Cardiovasc. Eng. Technol* 5(2):189–201, 2014. [PubMed: 25050140]
27. Kung EO, Les AS, Figueroa CA, Medina F, Arcaute K, Wicker RB, McConnell MV, and Taylor CA. In vitro validation of finite element analysis of blood flow in deformable models. *Ann. Biomed. Eng* 39(7):1947–1960, 2011. [PubMed: 21404126]
28. Kwak BR, Bäck M, Bochaton-Piallat M-L, Caligiuri G, Daemen MJAP, Davies PF, Hofer IE, Holvoet P, Jo H, Krams R, et al. Biomechanical factors in atherosclerosis: mechanisms and clinical implications. *Eur. Heart J* 35(43):3013–3020, 2014. [PubMed: 25230814]
29. Les AS, Shadden SC, Figueroa CA, Park JM, Tedesco MM, Herfkens RJ, Dalman RL, and Taylor CA. Quantification of Hemodynamics in Abdominal Aortic Aneurysms During Rest and Exercise Using Magnetic Resonance Imaging and Computational Fluid DynamicsQuantification of hemodynamics in abdominal aortic aneurysms during rest and exercise using magnetic resonance imaging and computational fluid dynamics. *Ann. Biomed. Eng* 38(4):1288–1313, 2010. [PubMed: 20143263]
30. Li C, Huang R, Ding Z, Gatenby JC, Metaxas DN, and Gore JC. A level set method for image segmentation in the presence of intensity inhomogeneities with application to mri. *IEEE Trans. Image Process* 20(7):2007–2016, 2011. [PubMed: 21518662]
31. Lonyai A, Dubin AM, Feinstein JA, Taylor CA, and Shadden SC. New insights into pacemaker lead-induced venous occlusion: Simulation-based investigation of alterations in venous biomechanics. *Cardiovasc. Eng* 10(2):84–90, 2010. [PubMed: 20514553]
32. Lorigo LM, Faugeras OD, Grimson WEL, Keriven R, Kikinis R, Nabavi A, and Westin C-F. Curves: Curve evolution for vessel segmentation. *Med. Image Anal* 5(3):195–206, 2001. [PubMed: 11524226]
33. Malek AM, Alper SL, and Izumo S. Hemodynamic shear stress and its role in atherosclerosis. *JAMA* 282(21):2035–2042, 1999. [PubMed: 10591386]
34. Marsden AL, Bernstein AJ, Reddy VM, Shadden SC, Spilker RL, Chan FP, Taylor CA, and Feinstein JA. Evaluation of a novel Y-shaped extracardiac Fontan baffle using computational fluid dynamics. *J. Thorac. Cardiovasc. Surg* 137(2):394–U187, 2009. [PubMed: 19185159]
35. Marsden AL, and Esmaily-Moghadam M. Multiscale modeling of cardiovascular flows for clinical decision support. *Appl. Mech. Rev* 67(3):030804, 2015.

36. Marsden AL, Reddy VM, Shadden SC, Chan FP, Taylor CA, and Feinstein JA. A new multiparameter approach to computational simulation for Fontan assessment and redesign. *Congenit. Heart Dis* 5(2):104–117, 2010. [PubMed: 20412482]
37. Martin MH, Feinstein JA, Chan FP, Marsden AL, Yang W, and Reddy VM. Technical feasibility and intermediate outcomes of a hand-crafted, area-preserving, bifurcated “Y-Graft” Fontan. *Thorac. Cardiovasc. Surg* 149(1):247–255, 2015.
38. Merkow J, Tu Z, Kriegman D, and Marsden AL. Structural edge detection for cardiovascular modeling In: *International Conference on Medical Image Computing and Computer-Assisted Intervention*, pp. 735–742. Springer, New York, 2015.
39. Milner JS, Moore JA, Rutt BK, and Steinman DA. Hemodynamics of human carotid artery bifurcations: computational studies with models reconstructed from magnetic resonance imaging of normal subjects. *J. Vasc. Surg* 28(1):143–156, 1998. [PubMed: 9685141]
40. Moore JA, Steinman DA, Holdsworth DW, and Ethier CR. Accuracy of computational hemodynamics in complex arterial geometries reconstructed from magnetic resonance imaging. *Ann. Biomed. Eng* 27(1):32–41, 1999.
41. Morbiducci U, Kok AM, Kwak BR, Stone PH, Steinman DA, Wentzel JJ, et al. Atherosclerosis at arterial bifurcations: evidence for the role of haemodynamics and geometry. *Thromb. Haemost* 115(3):484–492, 2016. [PubMed: 26740210]
42. Morgan VL, Roselli RJ, and Lorenz CH. Normal three-dimensional pulmonary artery flow determined by phase contrast magnetic resonance imaging. *Ann. Biomed. Eng* 26(4):557–566, 1998. [PubMed: 9662148]
43. Mukherjee D, Jani ND, Selvaganesan K, Weng CL, and Shadden SC. Computational assessment of the relation between embolism source and embolus distribution to the circle of Willis for improved understanding of stroke etiology. *J. Biomech. Eng* 138(8):081008–1–081008–13, 2016.
44. Mukherjee D, Padilla J, and Shadden SC. Numerical investigation of fluid-particle interactions for embolic stroke. *Theor. Comput. Fluid Dyn* 30(1):23–39, 2016.
45. Nichols W, O’Rourke M, and Vlachopoulos C. *McDonald’s Blood Flow in Arteries: Theoretical, Experimental and Clinical Principles*. CRC Press, Boca Raton, 2011.
46. Oakes JM, Marsden AL, Grandmont C, Shadden SC, Darquenne C, and Vignon-Clementel IE. Airflow and particle deposition simulations in health and emphysema: from in vivo to in silico animal experiments. *Ann. Biomed. Eng* 42(4):899–914, 2014. [PubMed: 24318192]
47. Olufsen MS, Peskin CS, Kim WY, Pedersen EM, Nadim A, and Larsen J. Numerical simulation and experimental validation of blood flow in arteries with structured-tree outflow conditions. *Ann. Biomed. Eng* 28(11):1281–1299, 2000. [PubMed: 11212947]
48. Perktold K, Hofer M, Karner G, Trubel W, and Schima H. Computer simulation of vascular fluid dynamics and mass transport: optimal design of arterial bypass anastomoses. *Proc. ECCOMAS* 98:484–489, 1998.
49. Ramachandra AB, Kahn AM, and Marsden AL. Patient-specific simulations reveal significant differences in mechanical stimuli in venous and arterial coronary grafts. *J. Cardiovasc. Transl. Res* 9(4):279–290, 2016. [PubMed: 27447176]
50. Roccabianca S, Figueroa CA, Tellides G, and Humphrey JD. Quantification of regional differences in aortic stiffness in the aging human. *J. Mech. Behav. Biomed. Mater* 29:618–634, 2014. [PubMed: 23499251]
51. Sahni O, Müller J, Jansen KE, Shephard MS, and Taylor CA. Efficient anisotropic adaptive discretization of the cardiovascular system. *Comput. Methods Appl. Mech. Eng* 195(41–43):5634–5655, 8 2006.
52. Sankaran S, Esmaily-Moghadam M, Kahn AM, Guccione J, Tseng E, and Marsden AL. Patient-specific multiscale modeling of blood flow for coronary artery bypass graft surgery. *Ann. Biomed. Eng* 40(1):2228–2242, 2012. [PubMed: 22539149]
53. Schiavazzi DE, Arbia G, Baker C, Hlavacek AM, Hsia TY, Marsden AL, Vignon-Clementel IE, and The Modeling of Congenital Hearts Alliance (MOCHA) Investigators. Uncertainty quantification in virtual surgery hemodynamics predictions for single ventricle palliation. *Int. J. Numer. Methods Biomed. Eng* 32(3), 2016.

54. Schiavazzi DE, Kung EO, Marsden AL, Baker C, Pennati G, Hsia T-Y, Hlavacek A, Dorfman AL and Modeling of Congenital Hearts Alliance (MOCHA) Investigators et al. Hemodynamic effects of left pulmonary artery stenosis after superior cavopulmonary connection: a patient-specific multiscale modeling study. *J. Thorac. Cardiovasc. Surg* 149(3):689–696, 2015. [PubMed: 25659189]
55. Shadden SC, and Taylor CA. Characterization of coherent structures in the cardiovascular system. *Ann. Biomed. Eng* 36:1152–1162, 2008. [PubMed: 18437573]
56. Steinman DA, Hoi Y, Fahy P, Morris L, Walsh MT, Aristokleous N, Anayiotos AS, Papaharilaou Y, Arzani A, Shadden SC, et al. Variability of computational fluid dynamics solutions for pressure and flow in a giant aneurysm: the ASME 2012 Summer Bioengineering Conference CFD Challenge. *J. Biomech. Eng* 135(2):021016, 2013. [PubMed: 23445061]
57. Suh GY, Les AS, Tenforde AS, Shadden SC, Spilker RL, Yeung JJ, Cheng CP, Herfkens RJ, Dalman RL, and Taylor CA. Quantification of particle residence time in abdominal aortic aneurysms using magnetic resonance imaging and computational fluid dynamics. *Ann. Biomed. Eng* 39:864–883, 2011. [PubMed: 21103933]
58. Suh GY, Tenforde AS, Shadden SC, Spilker RL, Cheng CP, Herfkens RJ, Dalman RL, and Taylor CA. Hemodynamic changes in abdominal aortic aneurysms with increasing exercise intensity using MR exercise imaging and image-based computational fluid dynamics. *Ann. Biomed. Eng* 39:2186–2202, 2011. [PubMed: 21509633]
59. Tang BT, Pickard SS, Chan FP, Tsao PS, Taylor CA, and Feinstein JA. Wall shear stress is decreased in the pulmonary arteries of patients with pulmonary arterial hypertension: an image-based, computational fluid dynamics study. *Pulm. Circ* 2(4):470–476, 2012. [PubMed: 23372931]
60. Taylor CA, Draney MT, Ku JP, Parker D, Steele BN, Wang K, and Zarins CK. Predictive medicine: computational techniques in therapeutic decision-making. *Comput. Aided Surg* 4(5):231–247, 1999. [PubMed: 10581521]
61. Taylor CA, Fonte TA, and Min JK. Computational fluid dynamics applied to cardiac computed tomography for noninvasive quantification of fractional flow reserve: scientific basis. *J. Am. Coll. Cardiol* 61(22):2233–2241, 2013. [PubMed: 23562923]
62. Taylor CA, Hughes TJR, and Zarins CK. Computational investigations in vascular disease. *Comput. Phys* 10(3):224–232, 1996.
63. Taylor CA, Hughes TJR, and Zarins CK. Finite element modeling of blood flow in arteries. *Comput. Methods Appl. Mech. Eng* 158(1):155–196, 1998.
64. Tran JS, Schiavazzi DE, Ramachandra AB, Kahn AM, and Marsden AL. Automated tuning for parameter identification and uncertainty quantification in multi-scale coronary simulations. *Comput. Fluids*, 2016.
65. Updegrove A, Wilson NM, and Shadden SC. Boolean and smoothing of discrete polygonal surfaces. *Adv. Eng. Softw* 95:16–27, 2016.
66. Vignon-Clementel IE, Figueroa CA, Jansen KE, and Taylor CA. Outflow boundary conditions for three-dimensional finite element modeling of blood flow and pressure in arteries. *Comput. Methods Appl. Mech. Eng* 195(29–32):3776–3796, 2006.
67. Wang KCY Level set methods for computational prototyping with application to hemodynamic modeling PhD thesis, Stanford University, 2001.
68. Wentzel JJ, Janssen E, Vos J, Schuurbijs JCH, Krams R, Serruys PW, de Feyter PJ, and Slager CJ. Extension of increased atherosclerotic wall thickness into high shear stress regions is associated with loss of compensatory remodeling. *Circulation* 108(1):17–23, 2003. [PubMed: 12821552]
69. Whiting CH, and Jansen KE. A stabilized finite element method for the incompressible Navier-Stokes equations using a hierarchical basis. *Int. J. Numer. Methods Fluids* 35(1):93–116, 2001.
70. Wilson NM, Arko FR, and Taylor CA. Predicting changes in blood flow in patient-specific operative plans for treating aortoiliac occlusive disease. *Comput. Aided Surg* 10(4):257–277, 2005. [PubMed: 16393794]
71. Yang W, Chan FP, Reddy VM, Marsden AL, and Feinstein JA. Flow simulations and validation for the first cohort of patients undergoing the Y-graft Fontan procedure. *J. Thorac. Cardiovasc. Surg* 149(1):247–255, 2015.

72. Zhou M, Sahni O, Kim HJ, Figueroa CA, Taylor CA, Shephard MS, and Jansen KE. Cardiovascular flow simulation at extreme scale. *Comput. Mech*, 46(1):71–82, 2010.

Author Manuscript

Author Manuscript

Author Manuscript

Author Manuscript

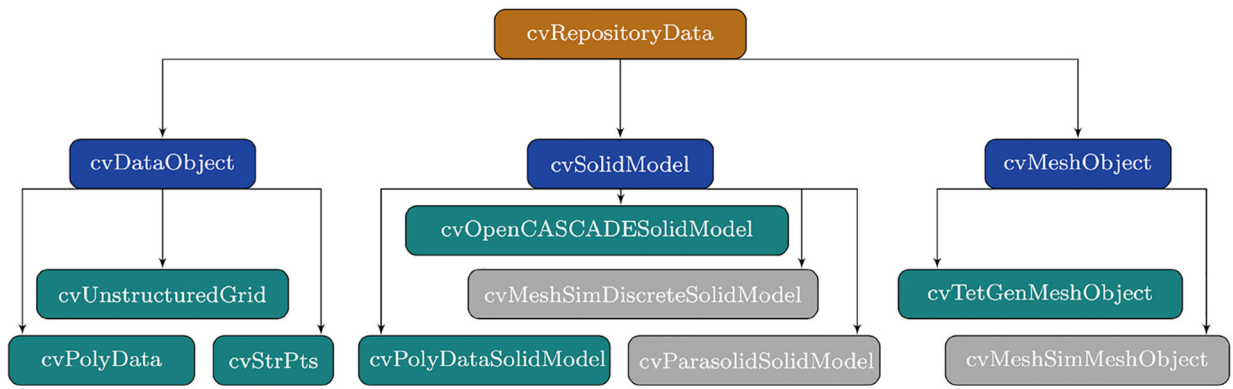


FIGURE 1. Inheritance diagram of *cvRepositoryData*. Derived classes in aqua are open source while derived classes in gray are commercial and optional.

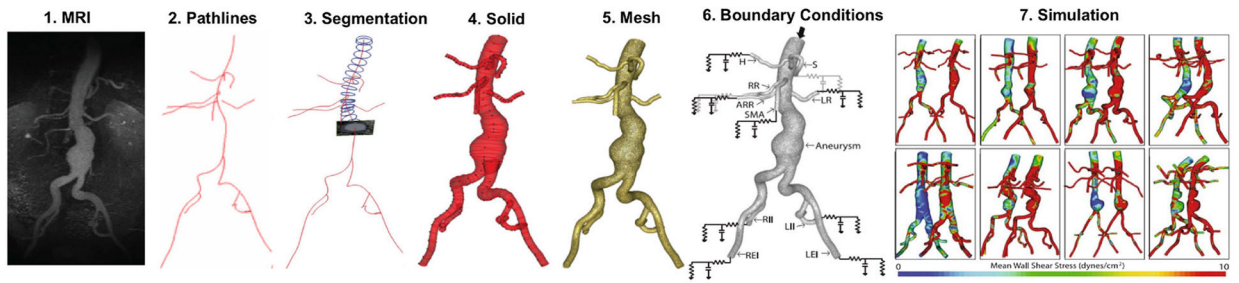


FIGURE 2.

The SimVascular pipeline leads the user from visualization of image data through to completion of blood flow simulations. Steps 2–4 correspond to the lofted 2D segmentation process. Adapted from Ref. 29.

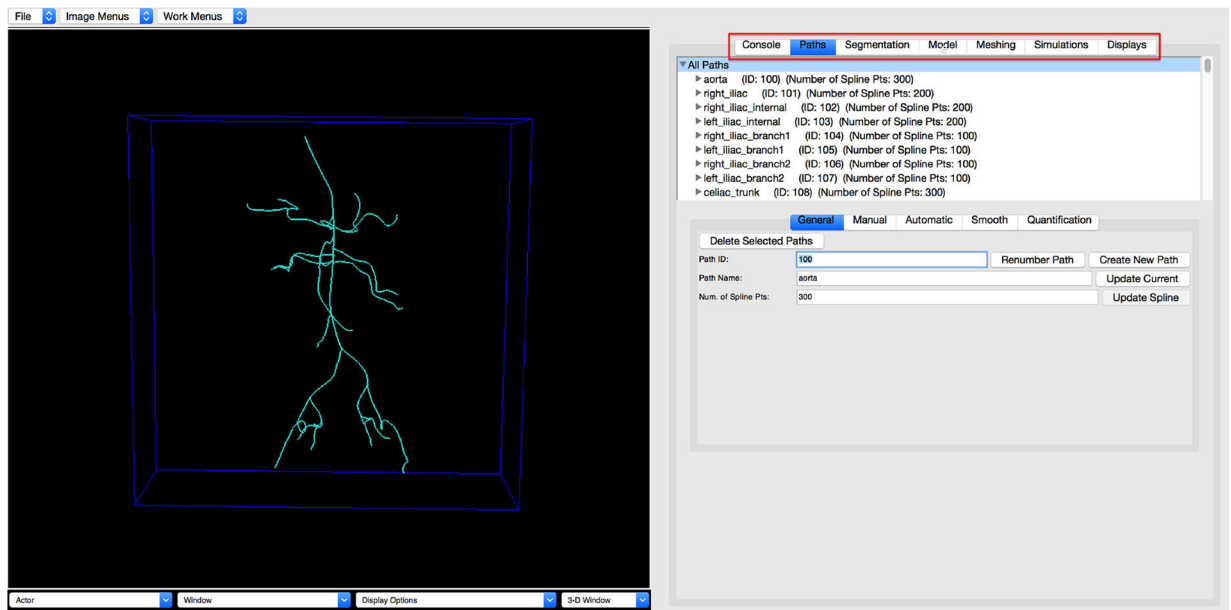


FIGURE 3.

The SimVascular pipeline is mirrored in the main work tabs of the GUI (enclosed in red box). Paths → Segmentation → Model → Meshing → Simulations.

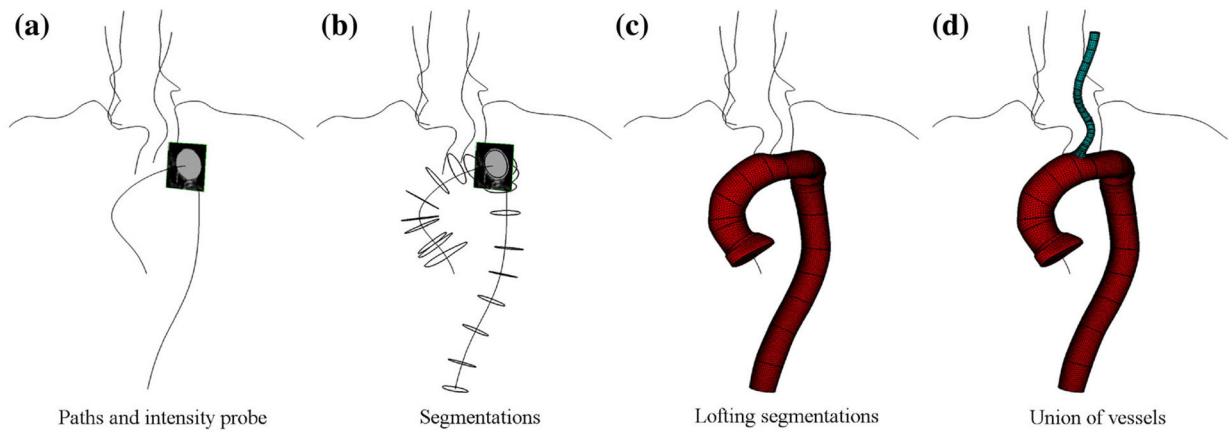


FIGURE 4.

Creation of a vascular geometry using the lofted 2D segmentation approach involves moving a cross-sectional image window along each vessel path (a) to create a series of segmentations (b) that are lofted to form each vessel (c). A solid model is generated by the union of individual vessel models (d).

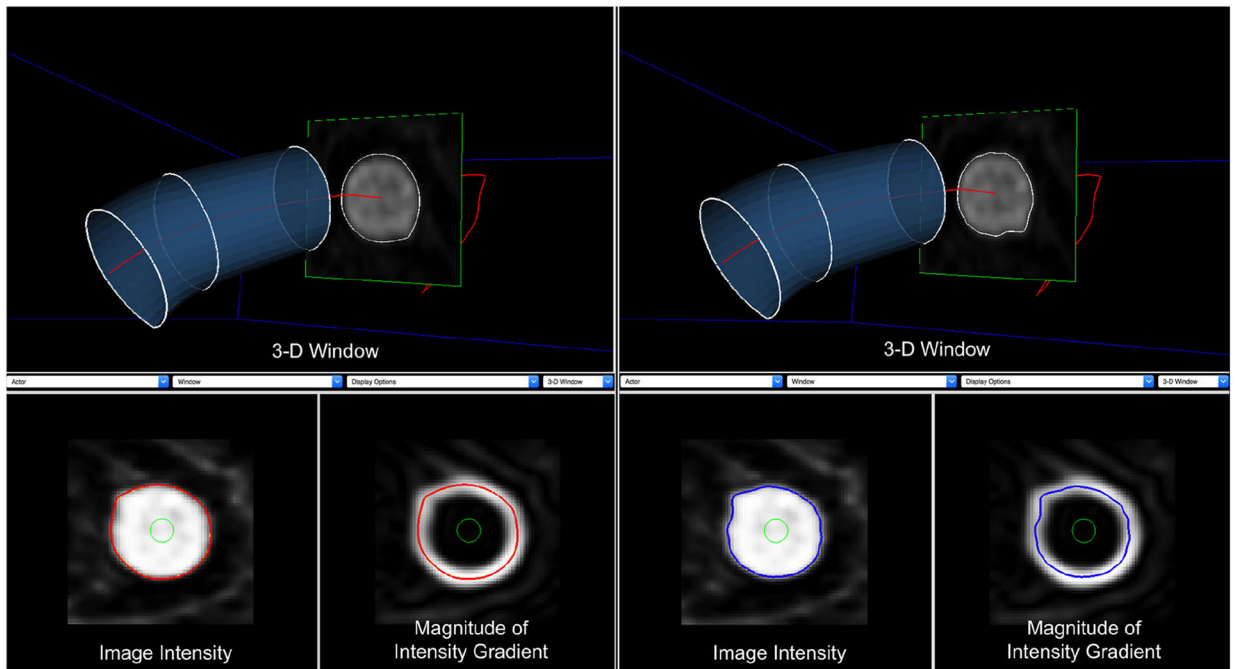


FIGURE 5.

Left: A slice along the vessel pathline is segmented using level set segmentation techniques.

Right: The same slice is segmented using threshold techniques.

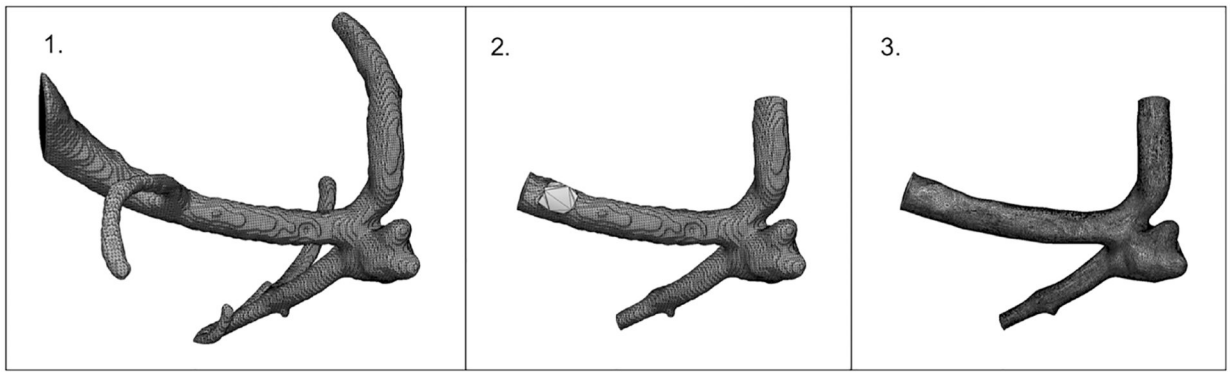


FIGURE 6.

A geometry imported into SimVascular and prepared for meshing using the PolyData solid model package. (1) The imported geometry (2) Extra and undesired portions of the geometry are removed and holes are filled (3) The geometry is smoothed, decimated, and subdivided.

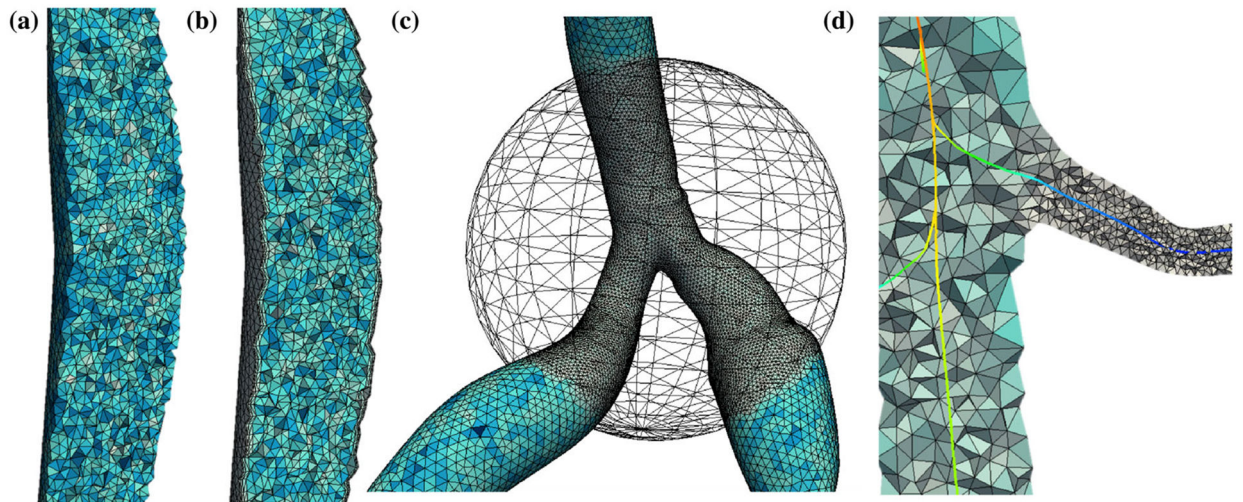


FIGURE 7.

A variety of meshing options are available in SimVascular. (a) Uniformly prescribed element size on mesh (b) Boundary layer mesh (c) Mesh with spherical refinement (d) Radius-based mesh.

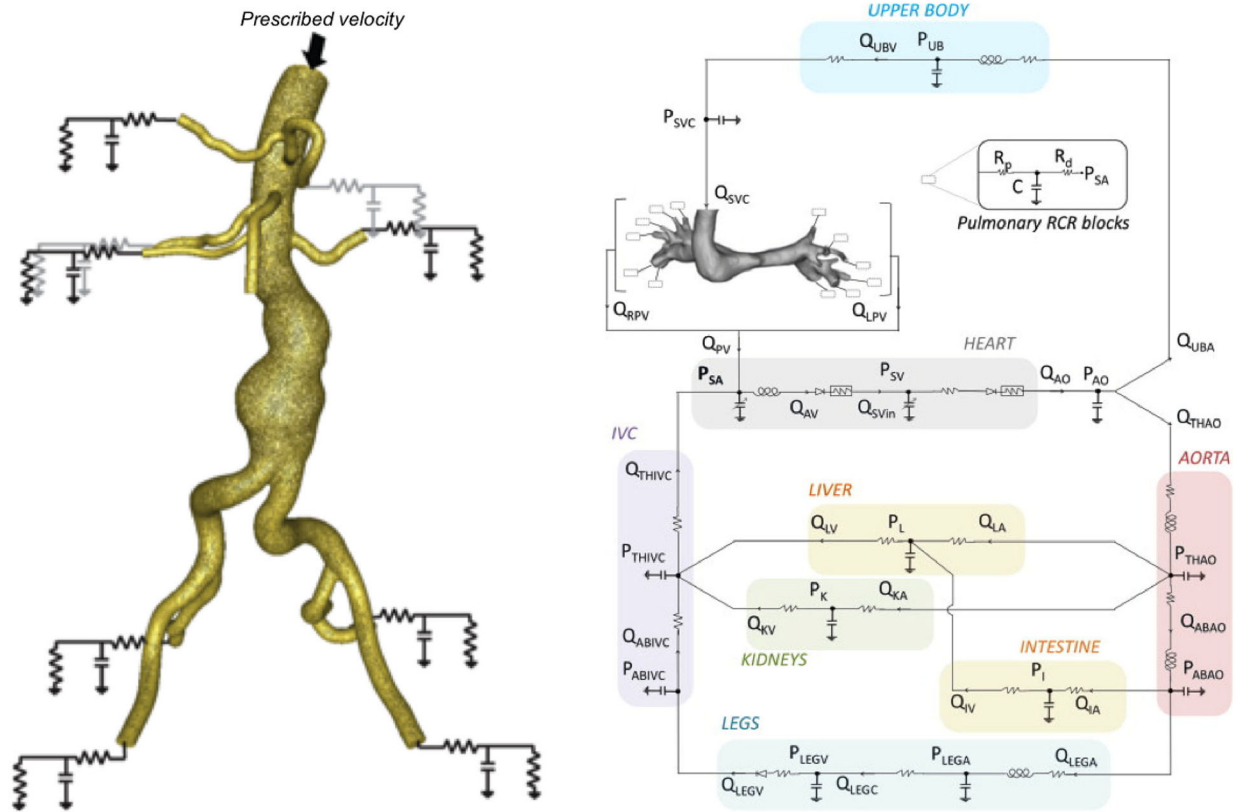


FIGURE 8. On the left, “open-loop” boundary conditions are prescribed on a model of an aorta (from Ref. 29). RCR circuits are applied to represent the downstream vasculature. On the right, “closed-loop” boundary conditions are applied to a Hemi-Fontan model (from Ref. 25).

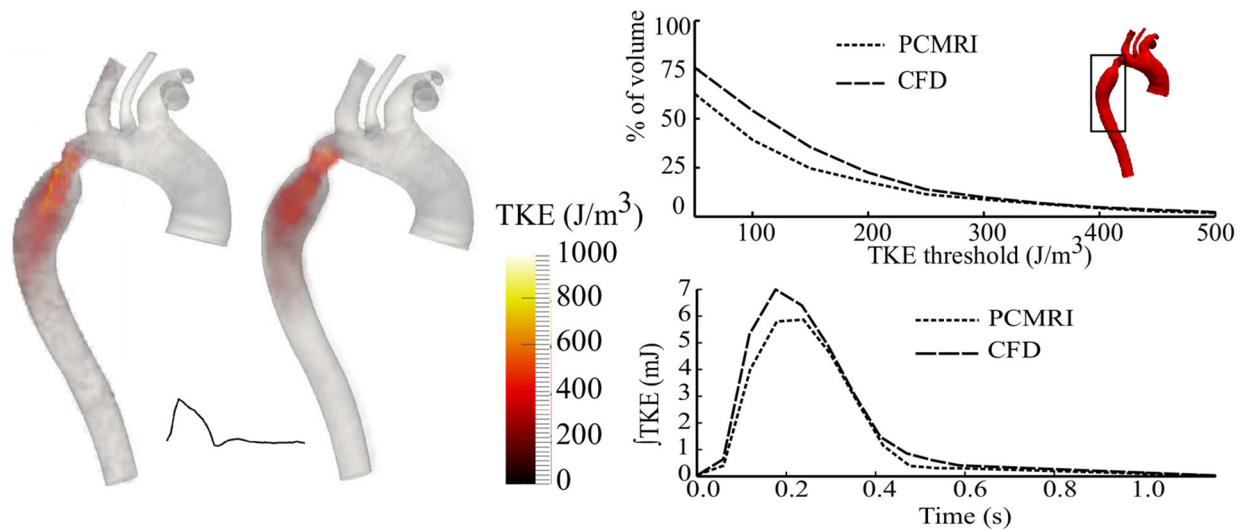


FIGURE 9.

In vivo validation of SimVascular's finite element flow solver for aortic coarctation. (left) Comparison of fluctuation intensity (TKE) fields from PCMRI and from SimVascular (CFD) during systole. (right, top) Percentage of the descending aorta (boxed region) with fluctuation intensity above various thresholds at systole. (right, bottom) Integral of the fluctuation intensity field over the descending aorta (boxed region) vs. time. Figures adapted from Ref. 1.

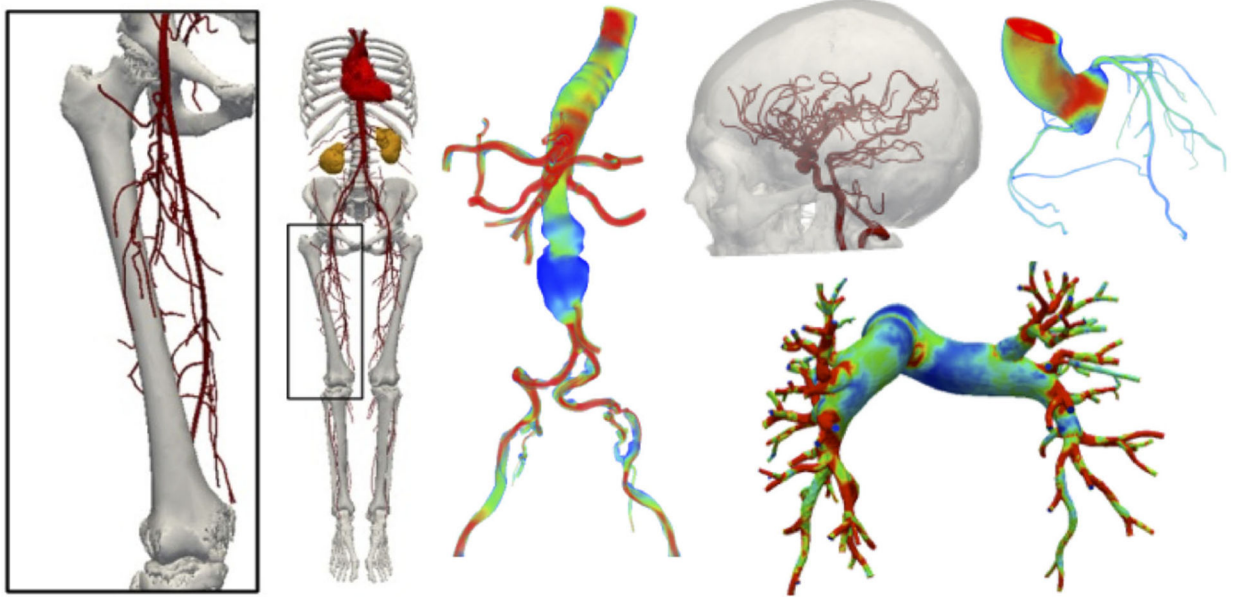


FIGURE 10.

A sampling of the wide variety of model categories and simulation results available online in the vascular model repository at <http://www.vascularmodel.com>.

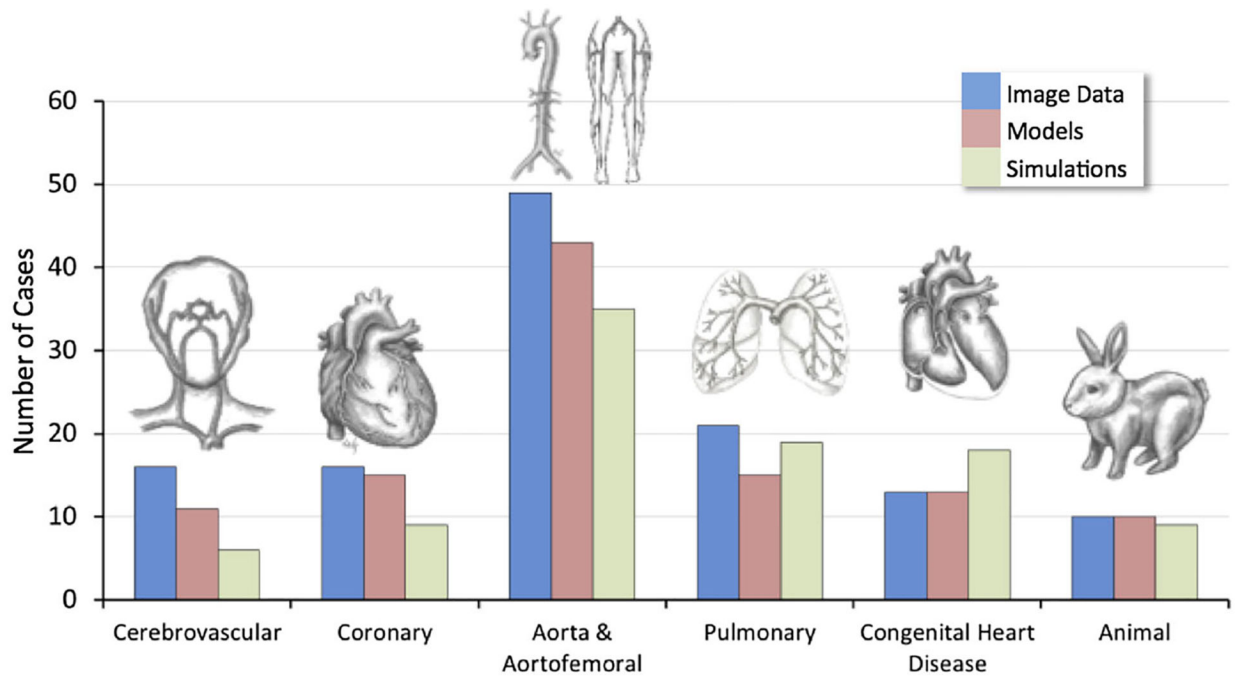


FIGURE 11. The vascular mode repository combines the results of over 100 studies of varying image data, model complexity, and simulation type.

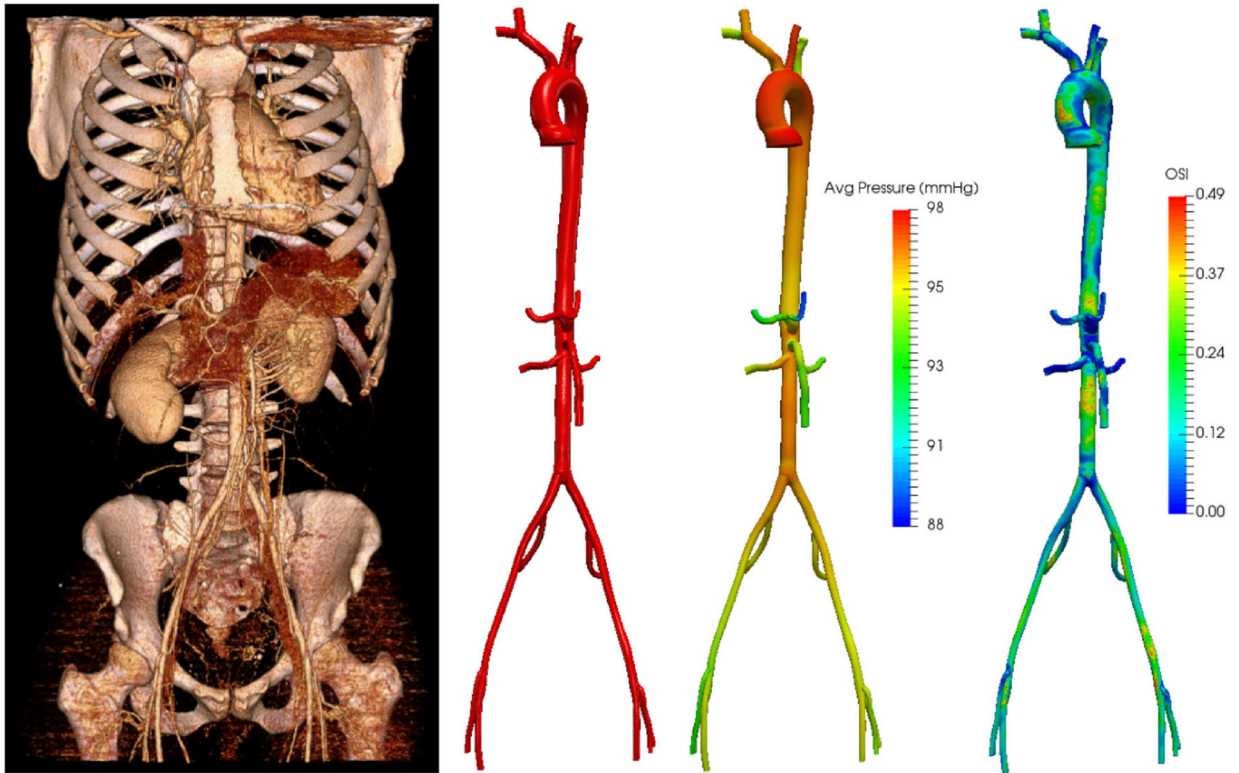


FIGURE 12.

The image volume and the constructed model for the aortic and femoral arteries of a 21 year old female (left two panels). Representative simulation results of the time-averaged pressure field and oscillatory shear index (OSI)²⁴ field are shown (right two panels).

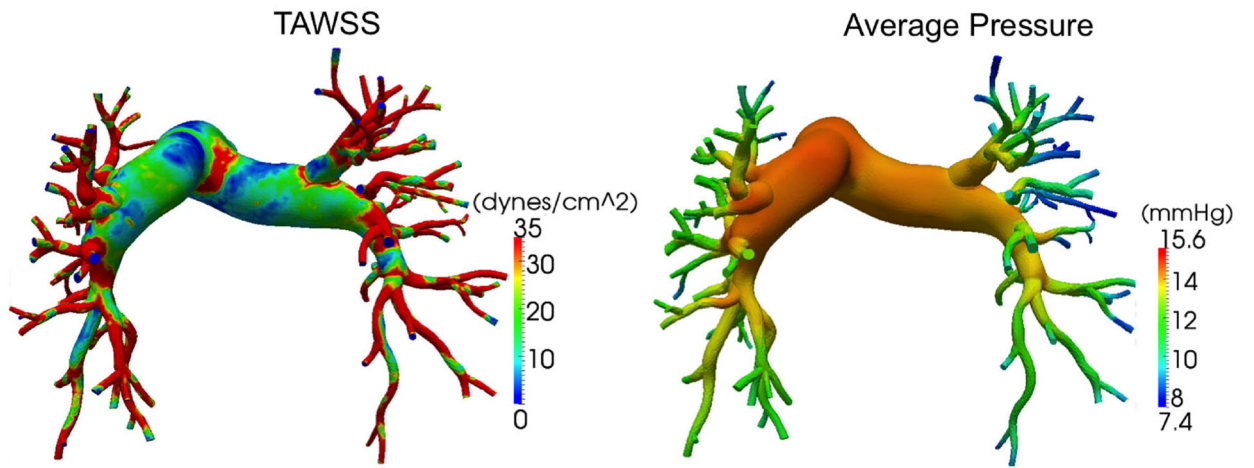


FIGURE 13. Time averaged wall shear stress and average pressure over one cardiac cycle for the pulmonary arteries of a 67 year old woman.

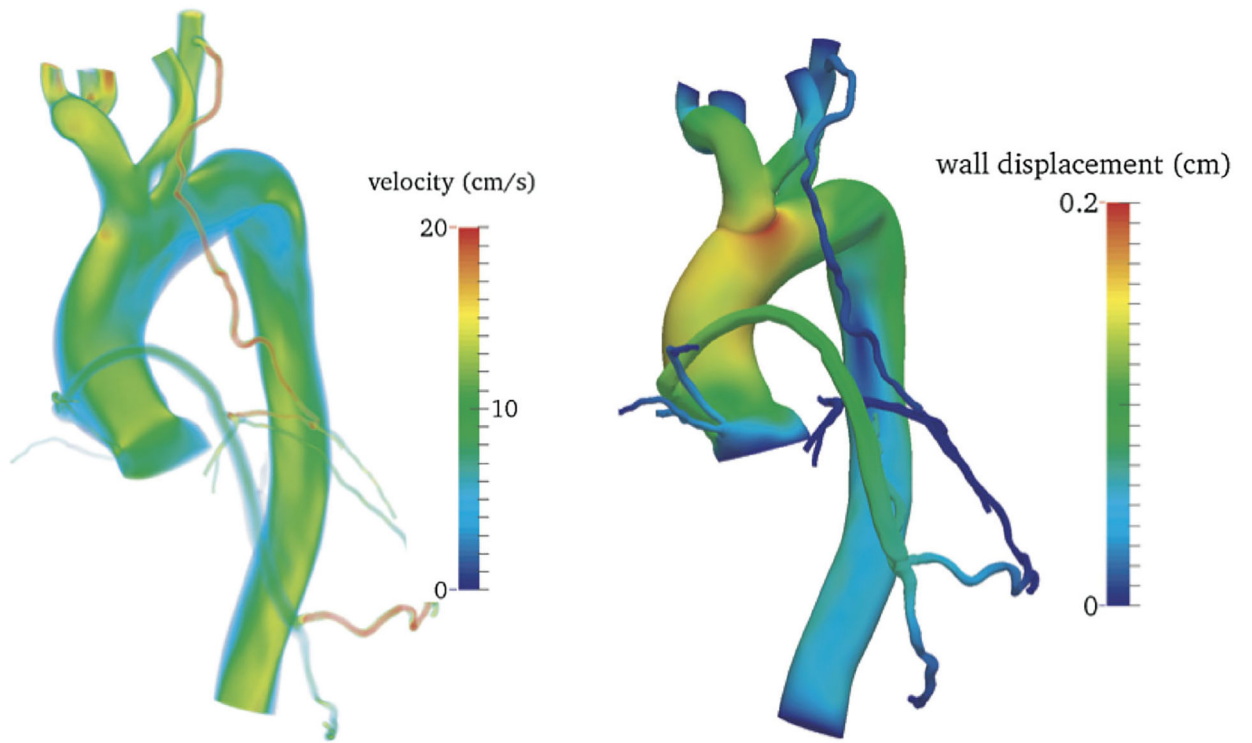


FIGURE 14. Model of the aorta, coronary arteries, and a bypass graft constructed from CT. Velocity magnitude volume render during end diastole (left) and wall displacements during peak systole calculated from FSI simulation (right). Adapted from Ref. 49.